This manuscript has been co-authored by UT-Battelle, LLC under Contract No. DE-AC05-00OR22725 with the U.S. Department of Energy. The United States Government retains and the publisher, by accepting the article for publication, acknowledges that the United States Government retains a non-exclusive, paid-up, irrevocable, world-wide license to publish or reproduce the published form of this manuscript, or allow others to do so, for United States Government purposes. The Department of Energy will provide public access to these results of federally sponsored research in accordance with the DOE Public Access Plan (http://energy.gov/downloads/doe-public-access-plan).

# K<sub>2</sub>CuX<sub>3</sub> (X= Cl, Br): All-Inorganic Lead-Free Blue Emitters with Near-Unity Photoluminescence Quantum Yield

Tielyr D. Creason, <sup>1</sup> Timothy M. McWhorter, <sup>1</sup> Zane Bell, <sup>2</sup> Mao-Hua Du<sup>3</sup> Bayrammurad Saparov <sup>1</sup>\*

<sup>1</sup>Department of Chemistry and Biochemistry, University of Oklahoma, 101 Stephenson Parkway, Norman, OK 73019, United States

<sup>2</sup>Isotope and Fuel Cycle Technology Division, Oak Ridge National Laboratory, Oak Ridge, Tennessee 37830, Unites States (presently retired)

<sup>3</sup>Materials Science & Technology Division, Oak Ridge National Laboratory, Oak Ridge, Tennessee 37830, United States

\*Corresponding Author: <a href="mailto:saparov@ou.edu">saparov@ou.edu</a>

ABSTRACT. Recently, copper(I) halides have been gaining increased attention as highly luminescent nontoxic alternatives to lead halide perovskites for optoelectronic applications. Here, we report preparation of blue emitting, lead free, all-inorganic halides  $K_2CuX_3$  (X=Cl, Br) through five synthetic methods including traditional solid-state and solution methods. The photoluminescence (PL) emission spectra of  $K_2CuCl_3$  and  $K_2CuBr_3$  exhibit narrow peaks centered at 392 nm and 388 nm with full widths at half maximum (FWHM) values of ~54 nm. The visible bright blue emission is corroborated by the remarkably high photoluminescence quantum yield (PLQY) values up to ~97%. Furthermore, radioluminescence measurements on  $K_2CuCl_3$  yield a bright peak at 404 nm under irradiation with X rays at 200 kVp, 20 mA, which is optimal for use with PMTs and Si photomultipliers, suggesting a strong potential of this family for radiation detection applications. Based on our combined experimental and computational investigations, the origin of the efficient luminescence in  $K_2CuX_3$  is attributed to the high stability self-trapped excitons (STE) formed in the one-dimensional anionic  $\frac{1}{\omega}[CuX_3]^{2-}$  chains. Advantageously,  $K_2CuX_3$  demonstrate

improved air- and photostability compared to the previously reported copper(I) halides. The discovery of highly efficient and high stability light-emitters based on earth-abundant copper(I) halides paves the way for their potential practical applications.

#### INTRODUCTION

In the last few decades, significant efforts have been devoted to developing earth-abundant, luminescent materials and nanomaterials that demonstrate high stability and photoluminescence (PL) quantum yield.<sup>1-3</sup> Among these, multinary metal halides, especially halide perovskites and their structural derivatives, have been the focus of much attention owing to their high-efficiency white, blue, red and green emission.<sup>4-15</sup> Development of high-efficiency blue emitters has lagged compared to red and green emitters due to the higher energy optical transition required for obtaining blue emission.<sup>9, 16-19,</sup> Despite remarkable structural diversity and optoelectronic properties, lead halide perovskites have their own drawbacks such as poor air stability, photoinstability, and toxicity, which could prevent their commercialization.<sup>20-24</sup>

Recently, several families of copper halides emerged as promising alternatives to luminescent lead halides. These include near-unity green photoluminescence in Cs<sub>3</sub>Cu<sub>2</sub>Cl<sub>5</sub> and near-unity blue emission in Cs<sub>3</sub>Cu<sub>2</sub>X<sub>5</sub> (X = Br, I) and Rb<sub>2</sub>CuX<sub>3</sub> (X = Cl, Br), to name just a few.<sup>9, 25-28</sup> Tunable blue, green and yellow emission has also been observed for the CsCu<sub>2</sub>X<sub>3</sub> family, however, the measured photoluminescence quantum yield (PLQY) values are lower compared to the aforementioned families.<sup>29</sup> In all of these families, luminescence is attributed to the self-trapped excitons (STEs), which are induced by strong charge localization within low-dimensional crystal structures

of these copper halides. The formation of STEs is accompanied by a significant excited state structural reorganization, typically leading to a very strong room temperature photoluminescence (PL) emission with large Stokes shifts. Given the importance of structural distortions in light emission in metal halides, narrow structural changes can lead to a significant change in the observed luminescence behavior of materials. A recent high-pressure study of CsCu<sub>2</sub>I<sub>3</sub> confirms this conjecture as a remarkable enhancement of luminescence and changes in STE emission is observed for this material due to the structural evolution of the material under pressure.<sup>30</sup>

Here, we report the preparation and characterization of K<sub>2</sub>CuX<sub>3</sub> (X= Cl, Br), which are the chemically pressurized form of the bright blue emitting Rb<sub>2</sub>CuX<sub>3</sub>. <sup>9, 26, 27</sup> Along with the bright blue emission, Rb<sub>2</sub>CuX<sub>3</sub> have recently shown a strong potential as sensitive X-ray scintillator materials. 26, 27 Despite their excellent fundamental optical properties, Rb<sub>2</sub>CuX<sub>3</sub> contain intrinsically radiactive Rb and the photostability of Rb<sub>2</sub>CuX<sub>3</sub> is poor with a reported ~75% drop in PLQY in only an hour of UV exposure. 9,27 In contrast, K<sub>2</sub>CuX<sub>3</sub> reported in this work show markedly improved air stability and photostability while preserving their ultrabright blue emission behavior. In this work,  $K_2CuX_3(X = Cl, Br)$  single crystals and polycrystalline powders were prepared via five different preparation methods including traditional solid-state methods, flux growth, slow cooling of a saturated solution, liquid-liquid diffusion, and liquid-vapor diffusion. Structural characterizations were performed using powder and single crystal X-ray diffraction methods. Optical properties of K<sub>2</sub>CuX<sub>3</sub> were studied using a combined computational and experimental approach through photoluminescence spectroscopy and density functional theory (DFT) methods. This work highlights the strong potential of inexpensive and earth-abundant copper halides for practical applications, which can be further fine-tuned through chemical substitution experiments.

#### EXPERIMENTAL SECTION

**Materials and Methods.** The starting reactants: potassium chloride (99%, J.T. Baker), copper(I) chloride (>99%, Sigma-Aldrich), potassium bromide (99%, Sigma-Aldrich) and copper(I) bromide (>99%, Alfa Aesar) were used as received. For high temperature synthesis experiments, the fused silica tubes were first annealed at 300 °C for 2 hours before quickly transferring to a nitrogen filled glovebox for long term storage. All manipulations of reactants and products were performed in a nitrogen-filled glovebox.

Polycrystalline Powders of K<sub>2</sub>CuX<sub>3</sub>. Polycrystalline powder samples of K<sub>2</sub>CuX<sub>3</sub> (X= Cl, Br) were prepared by grinding a 2:1 stoichiometric amount of KX and CuX for approximately 30 minutes under a nitrogen atmosphere. Then, the mixtures were pressed into pellets and sealed under vacuum in quartz tubes. The sealed ampoules were heated to 210 °C over the course of 4 hours, held at this temperature for 72 hours and cooled to room temperature over 18 hours. Each sample goes through this heating and cooling cycle at least twice, with a grinding in between, to ensure the complete consumption of reactants.

Flux growth of K<sub>2</sub>CuCl<sub>3</sub> Single Crystals. For single crystal growth experiments using molten salt as flux, a 21:29 molar ratio of KCl and CuCl were ground for approximately 30 minutes under a nitrogen atmosphere. The mixtures were then loaded into alumina crucibles. The crucibles were sealed inside evacuated quartz ampoules and placed into a furnace. The reaction mixtures were heated to 300 °C over 4 hours, held at this temperature for 10 hours, cooled to 170 °C over 130 hours and at this temperature for 336 hours. The liquid flux was removed via centrifugation and single crystals of K<sub>2</sub>CuCl<sub>3</sub> were isolated.

**K**<sub>2</sub>CuCl<sub>3</sub> Single Crystals via Slow Cooling of a Saturated Solution. K<sub>2</sub>CuCl<sub>3</sub> single crystals of up to 20 mm in length with 1 mm in diameter were prepared by mixing stoichiometric amounts of KCl and CuCl in a 6M HCl solution. In order to prevent oxidation, samples were loaded in a nitrogen glovebox and sealed with white rubber Suba-Seal septa. A Schlenk line was used with an oil bubbler to constantly flow nitrogen over the samples. Approximately 5% by volume H<sub>3</sub>PO<sub>2</sub>, was added to the KCl solution. Both solutions were heated at 100 °C until fully dissolved and clear. The CuCl solution was added dropwise to the KCl solution and allowed to mix for 1 hour. The samples were then cooled to room temperature for 6 hours. Colorless needle crystals of K<sub>2</sub>CuCl<sub>3</sub> were collected and washed in methanol.

Liquid-Liquid Diffusion Growth of K<sub>2</sub>CuBr<sub>3</sub> Single Crystals. K<sub>2</sub>CuBr<sub>3</sub> single crystals of up to 1 cm in lengths were prepared by mixing stoichiometric amounts of KBr and CuBr in a 4M HBr solution. In order to prevent oxidation samples were loaded in a nitrogen glovebox and sealed with white rubber Suba-Seal septa. A Schlenk line was used with an oil bubbler to constantly flow nitrogen over the samples. Approximately 10% by volume H<sub>3</sub>PO<sub>2</sub> was added to the KBr solution. Both solutions were fully dissolved and clear at room temperature. The CuBr was then added dropwise to KBr and the solutions were mixed for 1 hour at room temperature. An equal volume of methanol to HBr was layered on top of the HBr solution. Long (up to 1 cm) colorless needle crystals grew overnight, which were collected and washed in methanol.

Vapor-Liquid Diffusion Growth of K<sub>2</sub>CuBr<sub>3</sub> Single Crystals. K<sub>2</sub>CuBr<sub>3</sub> single crystals of 0.5 cm in size were prepared by mixing stoichiometric amounts of KBr and CuBr in a 4M HBr solution. In order to prevent oxidation, samples were loaded in a nitrogen glovebox and sealed with white rubber Suba-Seal septa. A Schlenk line was used with an oil bubbler to constantly flow

nitrogen over the samples. Approximately 10% by volume H<sub>3</sub>PO<sub>2</sub> was added to the KBr solution. Both solutions were fully dissolved and clear at room temperature. The CuBr was then added dropwise to KBr and the solutions were mixed for 1 hour at room temperature. The sample was then transferred to a test tube which was suspended from the top of a sealed glass jar with excess methanol at the bottom. The jar was placed in an oil bath at 60 °C, where 0.5 cm crystals grew over the course of 5 days. Crystals were washed in methanol.

Powder X-ray Diffraction (PXRD) Measurements. In order to establish bulk purity of samples, PXRD measurements were periodically taken on a Rigaku Miniflex600 equipped with D/tex detector and a Ni-filtered Cu-Kα radiation source. Data were collected at room temperature in the 3–90° (2θ) range, with a step size of 0.02°. The obtained PXRD patters were refined using the decomposition method. To test the air-stability of K<sub>2</sub>CuX<sub>3</sub>, powdered samples were left on a laboratory bench under ambient conditions (thermostat set at 20 °C and relative humidity of 30%) and periodic PXRD experiments were performed to monitor the changes. To quantify the sample composition changes, the Reference Intensity Ratio (RIR) quantitative analysis was performed using the PDXL2 program.

Single Crystal X-ray Diffraction (SCXRD). Single crystal X-ray diffraction (SXRD) data were collected on a Bruker D8 Quest with a Kappa geometry goniometer, an Incoatec Iµs X-ray source (graphite monochromated Mo-K $\alpha$  ( $\lambda$  = 0.71073 Å) radiation), and a Photon II detector. The data were corrected for absorption using the semiempirical method based on equivalent reflections, and the structures were solved by intrinsic phasing methods (SHELXT) as embedded in the APEX3 v2015.5-2 program. Site occupancy factors were checked by freeing occupancies of each unique crystallographic site. Details of the data collection and crystallographic parameters are

given in Table S1. Atomic coordinates, equivalent isotropic displacement parameters, and selected interatomic distances and bond angles are provided in Table S2 and Table S3 in the Supporting Information (SI). Additional information on the crystals structures investigations can be obtained in the form of a Crystallographic Information File (CIF), which were deposited in the Cambridge Crystallographic Data Centre (CCDC) database (deposition numbers 1989799 and 1989800)

Thermogravimetry and Differential Scanning Calorimetry (TGA/DSC) Measurements. Simultaneous thermogravimetric analysis and differential scanning calorimetry (TGA/DSC) were measured on ~15 mg of polycrystalline powder of K<sub>2</sub>CuX<sub>3</sub> on a TA Instruments SDT 650 thermal analyzer system. Sample was heated up from 25 to 475 °C under an inert flow of dry nitrogen gas at a rate of 100 mL/min, with a heating rate of 5 °C/min.

**Optical Measurements.** Room temperature photoluminescence emission (PL) and photoluminescence excitation (PLE) measurements were performed on polycrystalline powders of K<sub>2</sub>CuX<sub>3</sub> (X = Cl, Br) and single crystals of K<sub>2</sub>CuCl<sub>3</sub> on a Jobin Yvon Fluorolog-3 spectrofluorometer (HORIBA company) equipped with a Xenon lamp and a Quanta-φ integrating sphere using the two-curve method in a varied range from 280 to 860 nm. For lifetime measurements, a Time-Correlated Single Photon Counting (TCSPC) system including a DeltaHub DH-HT high throughput TCSPC controller and NanoLED NL-C2 pulsed diode controller was used. For light source, a 299 nm NanoLED diode was selected, which has a <1.2 ns pulse duration.

Photoluminescence quantum yield was determined by:

Quantum Yield = 
$$\left(\frac{Em_s - Em_b}{Ex_b - Ex_s}\right) * 100$$

where Ex<sub>s</sub> and Ex<sub>b</sub> are the integrated excitation profiles of the sample and the blank and Em<sub>s</sub> and Em<sub>b</sub> are the integrated emission profiles of the sample and blank respectively. An Area Balance Factor is applied in the FluorEssence software which accounts for changes in integration times between excitation and emission scans and for the use of neutral density filters. For the photostability measurement, a polycrystalline K<sub>2</sub>CuCl<sub>3</sub> sample was placed inside the Quanta-φ integrating sphere on the Jobin Yvon Fluorolog-3 spectrofluorometer. The sample was then exposed to the full power of the Xenon lamp of the spectrofluorometer at its PL excitation maximum of 291 nm. Periodic PLQY measurements were taken every 5 minutes under these conditions for a total of 60 minutes.

For radioluminescence (RL) measurements, a K<sub>2</sub>CuCl<sub>3</sub> polycrystalline pellet sample with ~5 × 5 × 3 mm<sup>3</sup> dimensions was fixed on a wooden stick using silicone optical grease (Bicron BC-630), and placed in an X-ray beam at the focal point of the optics of a Princeton Instruments Acton SP2150 UV-VIS spectrometer (see Figure S1) housed in the lead-lined irradiation cabinet. This instrument uses a Hamamatsu R928 photomultiplier tube (PMT) to receive light from a diffraction grating and mirror system scanned to cover the range from 200 to 650 nm. Data were collected as a function of wavelength at increments of 2 nm under irradiation with bremsstrahlung X rays at 200 kVp, 20 ma (~25 Gy/h). For each wavelength, 4 measurements were averaged with 250 ms integration time per measurement to reduce noise. For completeness, we ran an identical measurement of the wooden stick covered with optical grease to rule out the unlikely possibility that the grease was the source of the luminescence (Figure S2).

**Computational Methods.** Our calculations were based on density functional theory (DFT) as implemented in the VASP code.<sup>31</sup> The kinetic energy cutoff of the plane-wave basis is 295 eV.

The projector augmented wave method was used to describe the interaction between ions and electrons.<sup>32</sup> Lattice parameters were fixed at the experimentally measured values while the atomic positions were optimized until the force on each atom is less than 0.02 eV/Å.

The electronic band structure and density of states (DOS) were calculated using Perdew-Burke-Ernzerhof (PBE) exchange-correlation functional. The band gaps were corrected and excitonic properties were studied by using the hybrid PBE0 functional. The inclusion of 25% Fock exchange in the PBE0 functional significantly improves the band gap energy and the description of charge localization in insulators. The total energy of an exciton was calculated by fixing the occupation numbers of the electron and hole-occupied eigenlevels [ $\Delta$  self-consistent field ( $\Delta$ SCF) method PE0 functional energy differences between the excited and the ground states using PBE0-optimized ground-state and excited-state structures, respectively. The  $\Delta$ SCF method combined with the hybrid PBE0 functional allows excited-state structural relaxation and has shown accurate results in exciton excitation and emission energies in many low-dimensional metal halides and oxides, 45-49 including 1D and 0D copper halides. 9, 28, 50

## **RESULTS AND DISCUSSION**

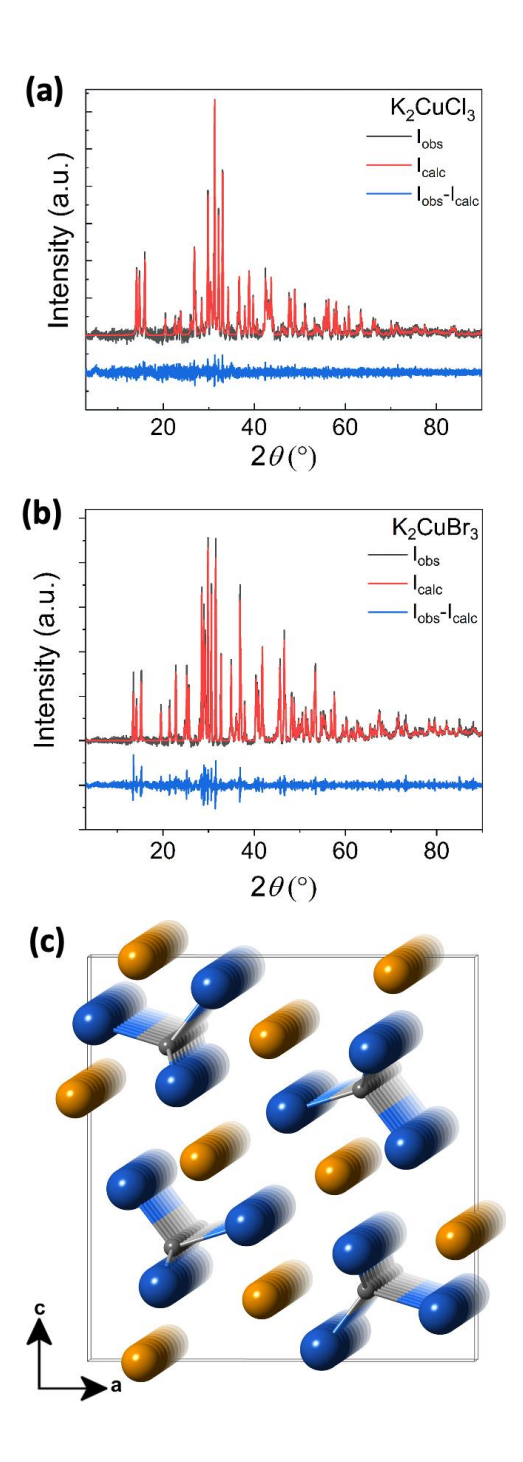


**Figure 1.** Room temperature PXRD patterns (black) fitted using the Pawley method (red) for (a)  $K_2CuCl_3$  and (b)  $K_2CuBr_3$  prepared using solid-state synthesis. (c) A ball-and-stick representation of the 1D crystal structure of  $K_2CuX_3$  viewed down the *b*-axis.

The optical photographs of single crystals and polycrystalline pellet of K<sub>2</sub>CuCl<sub>3</sub> and K<sub>2</sub>CuBr<sub>3</sub> obtained using solid-state heating, solution grown, liquid-liquid and liquid-vapor diffusion are illustrated in Figure S3. Such ease of preparation using multiple differing approaches can be advantageous for the potential practical applications of the K<sub>2</sub>CuX<sub>3</sub> compounds. Notably, the use of excess molten salt as a reactive flux is demonstrated for the first time for A<sub>2</sub>CuX<sub>3</sub> (A = K, Rb; X = Cl, Br) compounds. Although this approach produces high quality needle crystals of K<sub>2</sub>CuCl<sub>3</sub> (Figure S3), presence of dark-colored impurities and inclusions are noticeable due to a rapid oxidation of the surface CuCl self-flux.

To compare the purity and stability of samples prepared using various synthetic methods, we performed regular room temperature PXRD measurements; PXRD patterns of K2CuCl3 and K<sub>2</sub>CuBr<sub>3</sub> prepared using solid state synthesis approach are provided in Figure 1. As mentioned above, the flux-grown crystals of K<sub>2</sub>CuCl<sub>3</sub> form black impurity pieces when exposed to air. However, after an initial surface oxidation, no further noticeable changes occur for the flux-grown crystals. Single crystals of K<sub>2</sub>CuX<sub>3</sub> grown using the solution methods were also left in ambient air and showed no signs of degradation. In contrast, a polycrystalline powder sample of K<sub>2</sub>CuCl<sub>3</sub> prepared using solid-state synthesis and kept in ambient air shows signs of degradation after one day resulting in the formation of a small amount of KCuO impurity (Figure S4). There is a gradual increase of the KCuO impurity peak (up to estimated 6%) over a 2-months period. However, the crystallinity and peak intensities for K<sub>2</sub>CuCl<sub>3</sub> remain unchanged. Therefore, the formation of the KCuO impurity in powder samples exposed to the ambient lab environment are attributed to the oxidation of the leftover reactants in our samples. In fact, during our solid-state synthesis experiments, we noted that while smaller scale (total mass < 0.5g) reactions produce phase pure samples based on PXRD, larger scale reactions (total mass > 1 g) tend to show leftover reactant peaks in PXRD patterns. Thus, solid-state synthesis preparation of 1.5 g sample of K<sub>2</sub>CuBr<sub>3</sub> yielded a sample with a minor amount of unreacted CuBr impurity (~2%) after multiple grinding and annealing procedures (Figure S5). Unlike K<sub>2</sub>CuCl<sub>3</sub>, no change was noted for K<sub>2</sub>CuBr<sub>3</sub> over the three weeks tested. These results suggest that the K<sub>2</sub>CuBr<sub>3</sub> polycrystalline powders are stable under ambient air and moisture, whereas K<sub>2</sub>CuCl<sub>3</sub> samples show minor degradation due to the oxidation of left-over reactants. Notably, K<sub>2</sub>CuX<sub>3</sub> exhibit greatly improved air-stability compared to the heavier Rb<sub>2</sub>CuX<sub>3</sub> analogs. Thus, more than half (~56%) of a polycrystalline sample of Rb<sub>2</sub>CuCl<sub>3</sub> degraded forming RbCl and Rb<sub>2</sub>CuCl<sub>4</sub>·2H<sub>2</sub>O impurities when left in air under identical conditions for only a month.<sup>9</sup>

The results of SCXRD experiments are summarized in Tables S1-3.  $K_2CuX_3$  are isostructural with the previously reported  $Rb_2CuX_3^9$  and crystallize in the orthorhombic space group Pnma featuring  $1D_{\infty}^{-1}[CuX_3]^{2^-}$  chains separated by  $K^+$  cations (Figure 1c). The polyanionic  $_{\infty}^{-1}[CuX_3]^{2^-}$  are formed via corner sharing copper halide tetrahedra extending along the b-axis. The room temperature PXRD patterns of single crystals can be indexed based on the simulated pattern from the SCXRD data (Figures S6). The measured bond distances and angles within the  $1D_{\infty}^{-1}[CuX_3]^{2^-}$  chains in  $A_2CuX_3$  (A = K, Rb; X = Cl, Br) are similar (Table S3). Thus, the Cu-X bond distances are in the range 2.3319(4) - 2.3916(2) Å for  $K_2CuCl_3$ , nearly identical to the 2.3363(6) - 2.4243(3) Å range reported for  $Rb_2CuCl_3$ . For  $K_2CuBr_3$ , the Cu - X distances range from 2.4529(8) to 2.5215(4) Å; the Cu - Br bond lengths are longer than the Cu - Cl distances in accordance with the Shannon ionic radii trends for the halides. Si Since alkali metals are not directly involved in the optical transitions observed for the ternary alkali copper halides, and given the similarity in the  $1D_{\infty}^{-1}[CuX_3]^{2^-}$  ribbons, similar optical properties can be expected for  $K_2CuX_3$  and  $Rb_2CuX_3$ .

The thermal stability of K<sub>2</sub>CuCl<sub>3</sub> and K<sub>2</sub>CuBr<sub>3</sub> was evaluated by thermogravimetric analysis (TGA) and differential scanning calorimetry (DSC) measurements (Figure S7). Based on the TGA results, K<sub>2</sub>CuX<sub>3</sub> polycrystalline powder samples show no significant weight loss up to 460°C. These results are consistent with the improved thermal stability reported for all-inorganic metal halides such as Rb<sub>2</sub>CuCl<sub>3</sub>, Rb<sub>4</sub>Ag<sub>2</sub>BiBr<sub>9</sub>, Cs<sub>3</sub>Cu<sub>2</sub>Br<sub>5-x</sub>I<sub>x</sub>, Cs<sub>2</sub>SnI<sub>6</sub> etc. as compared to hybrid organic-inorganic metal halides.<sup>9, 28, 52, 53</sup> The obtained DSC results indicate a single thermal event for each sample, which have been assigned to the peritectic decompositions of K<sub>2</sub>CuCl<sub>3</sub> and K<sub>2</sub>CuBr<sub>3</sub> at 274 and 271 °C, respectively. These results are in a good agreement with the reported KX – CuX phase diagrams.<sup>54, 55</sup>

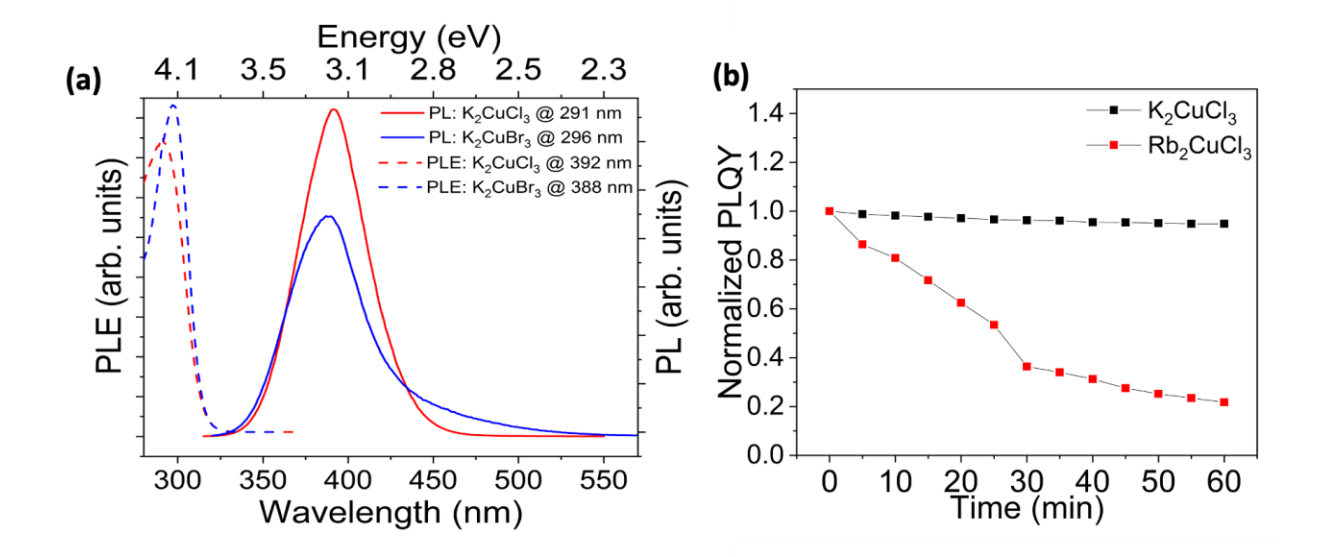


**Figure 2.** (a) Room temperature photoluminescence excitation (PLE) (dashed lines) and photoluminescence emission (PL) (solid lines) of polycrystalline powders of K<sub>2</sub>CuBr<sub>3</sub> (blue) and K<sub>2</sub>CuCl<sub>3</sub> (red). (b) A comparison of the normalized photoluminescent quantum yield (PLQY) of K<sub>2</sub>CuCl<sub>3</sub> (plotted in black) against that of Rb<sub>2</sub>CuCl<sub>3</sub>(plotted in red) under continuous irradiation suggests a significantly improved photostability of K<sub>2</sub>CuCl<sub>3</sub> compared to Rb<sub>2</sub>CuCl<sub>3</sub>.

The optical properties of as-synthesized K<sub>2</sub>CuX<sub>3</sub> were explored by photoluminescence spectroscopy. The photoluminescence excitation (PLE) and emission (PL) spectra for polycrystalline powders of K<sub>2</sub>CuCl<sub>3</sub> and K<sub>2</sub>CuBr<sub>3</sub> are provided in Figure 2a. A comparison between room temperature PL spectra for single crystals and polycrystalline powder samples of K<sub>2</sub>CuCl<sub>3</sub> is provided in Figure S8. Under UV irradiation, K<sub>2</sub>CuCl<sub>3</sub> and K<sub>2</sub>CuBr<sub>3</sub> show a bright blue emission with PL maxima at 392 and 388 nm, respectively. The corresponding PLE spectra for K<sub>2</sub>CuCl<sub>3</sub> and K<sub>2</sub>CuBr<sub>3</sub> show maxima at 291 and 296 nm, respectively. In combination, the measured PL and PLE peaks yield the Stokes shift values of 101 nm and 92 for K<sub>2</sub>CuCl<sub>3</sub> and K<sub>2</sub>CuBr<sub>3</sub>, respectively. The observed bright blue emission is attributed to the self-trapped excitons (STEs) in photoexcited K<sub>2</sub>CuX<sub>3</sub>.<sup>6,26</sup> For compounds with STE-based emission, the measured Stokes shifts of ~100 nm is relatively small as compared to other low-dimensional (1D and 0D) metal halides. <sup>49, 56, 57</sup> Furthermore, the measured PL peaks for K<sub>2</sub>CuX<sub>3</sub> are noticeably narrower with full width at half maximum (FWHM) ~ 54 nm compared to other STE based emitters including blue emitting copper halides such as Cs<sub>3</sub>Cu<sub>2</sub>Br<sub>5</sub> and Cs<sub>3</sub>Cu<sub>2</sub>I<sub>5</sub> (Table 1).<sup>9, 17, 27, 28</sup> Finally, blue emission with PLQY values of 96.58% and 55% measured for polycrystalline powder samples of K2CuCl3 and K2CuBr3, respectively, are among the highest reported to date. In combination, higher color purity blue emission with greater energy efficiency distinguishes the A<sub>2</sub>CuX<sub>3</sub> family from other known efficient blue emitters

**Table 1.** A comparison of the photophysical properties of high efficiency blue emitters based on all-inorganic copper halides<sup>9, 17, 27, 28</sup>

Compound	PLQY	PLmax	PLEmax	Stokes	FWHM	Ref
	(%)	(nm)	(nm)	shift (nm)	(nm)	
K <sub>2</sub> CuCl <sub>3</sub>	96.58	392	291	101	54	this work
K <sub>2</sub> CuBr <sub>3</sub>	55	388	296	92	54	this work
Rb <sub>2</sub> CuCl <sub>3</sub>	100	400	300	100	52	[9]
Rb <sub>2</sub> CuBr <sub>3</sub>	98.6	385	300	85	~54	[27]
Cs <sub>3</sub> Cu <sub>2</sub> I <sub>5</sub>	91.2	445	290	155	~175	[17]
Cs <sub>3</sub> Cu <sub>2</sub> Br <sub>5</sub>	50.1	455	298	157	75	[28]

Given the fact that K<sub>2</sub>CuX<sub>3</sub> are isostructural to Rb<sub>2</sub>CuX<sub>3</sub>, we attribute the mechanism of blue emission in K<sub>2</sub>CuX<sub>3</sub> to the highly stable STEs, which form upon the photoexcitation of these materials. The results of excitation-dependent and time-resolved PL measurements (Figure 3) further support the attribution of blue emission in K<sub>2</sub>CuX<sub>3</sub> to STEs. The observed excitation-dependent PL spectra are indicative of a single radiative transition mechanism (Figure 3a-b). From the time-resolved PL measurements a lifetime of 12.97 µs was extracted for K<sub>2</sub>CuCl<sub>3</sub> (Figure 3). This lifetime value is in a good agreement with the lifetime of 12.21 µs reported for Rb<sub>2</sub>CuCl<sub>3</sub>.<sup>9</sup> Interestingly, the measured optical properties of A<sub>2</sub>CuX<sub>3</sub> suggest a very weak dependence of PL properties on both the alkali A and halogen X sites (Table 1), which is in contrast to the observed significant changes in the PL properties of lead halides upon halogen substitution such as in case of the CsPbX<sub>3</sub> family.<sup>58</sup> Such unusually weak dependence of optical properties on the A and X sites in A<sub>2</sub>CuX<sub>3</sub> is due to the intricacies of their band structures (*vide infra*). Although the optical properties of Rb<sub>2</sub>CuX<sub>3</sub> and K<sub>2</sub>CuX<sub>3</sub> are similar, K<sub>2</sub>CuX<sub>3</sub> reported in this work are found to exhibit both greater air stability (*vide supra*) and photostability compared to Rb<sub>2</sub>CuX<sub>3</sub> (Figure 2b). One of the

key drawbacks of the high efficiency blue emitter Rb<sub>2</sub>CuCl<sub>3</sub>, for example, is that a 75% drop in PLQY is observed over the course of one hour under UV radiation.<sup>27</sup> In contrast, K<sub>2</sub>CuCl<sub>3</sub> shows only a 5% drop within the same time frame (Figure 2).

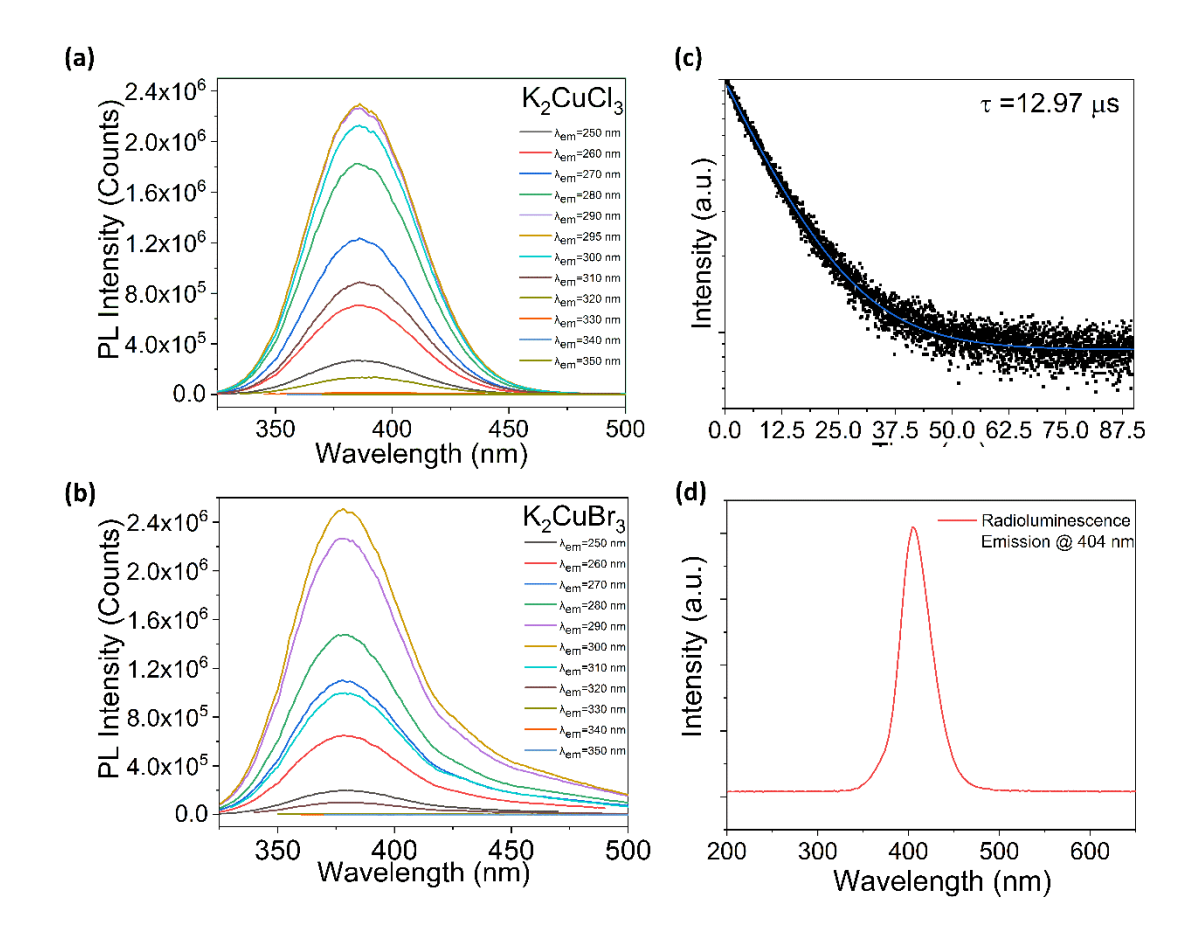


**Figure 3.** Excitation-dependent PL measurements for (a) K<sub>2</sub>CuCl<sub>3</sub> and (b) K<sub>2</sub>CuBr<sub>3</sub>. (c) Room temperature time-resolved PL spectrum for K<sub>2</sub>CuCl<sub>3</sub>. (d) A radioluminescence spectrum of K<sub>2</sub>CuCl<sub>3</sub> with emission centered at 404 nm.

In the literature, Rb<sub>2</sub>CuX<sub>3</sub> have been identified as potential materials for radiation detection applications.<sup>26, 27</sup> To evaluate the potential of K<sub>2</sub>CuX<sub>3</sub> for X-ray detection applications, we measured radioluminescence (RL) spectrum from a polycrystalline pellet of K<sub>2</sub>CuCl<sub>3</sub>. Under irradiation with bremsstrahlung X rays at 200 kVp, 20 ma (~25 Gy/h), the bright peak at 404 nm seen in

Figure 3d appeared. This peak in the same region as the room temperature PL emission under UV irradiation suggesting the same STE-based emission mechanism. The wavelength of the RL emission is optimal for use with PMTs and Si photomultipliers because these devices are optimized for the detection of light between 360 and 450 nm. Small samples, such as the one investigated here, are useful for the detection of  $\alpha/\beta$  radiation because the ranges of these particles in solid matter is small. The range of the 4.2 MeV alpha particles from  $^{238}$ U, is only  $\sim$ 20 µm (as calculated by the SRIM-2013 code) in K<sub>2</sub>CuCl<sub>3</sub>, making thin wafers, whether pressed polycrystalline material or single crystals, sufficient for efficient detection. <sup>59</sup> This form factor is suitable for health physics survey and ion beam instrumentation.

The considerations for X and gamma rays require accounting for the cross section for electromagnetic radiation causing the ejection of electrons and the range of electrons in K<sub>2</sub>CuCl<sub>3</sub>. The former determines the size of a compact or crystal needed for the efficient conversion of X and gamma rays to electrons, whereas the latter determines the efficiency with which ionization energy will be deposited in the crystal. Using photon cross section data available from NIST<sup>60</sup>, and the densities of analogous copper halides, the mean free paths of photons between 1 and 100 keV are shown in Figure 4 for K<sub>2</sub>CuCl<sub>3</sub>, K<sub>2</sub>CuBr<sub>3</sub>, Rb<sub>2</sub>CuCl<sub>3</sub>, and Rb<sub>2</sub>CuBr<sub>3</sub>. Based on our calculations, A<sub>2</sub>CuX<sub>3</sub> (A = K, Rb; X = Cl, Br) have similar X-ray absorption properties. Among these, K<sub>2</sub>CuCl<sub>3</sub> has the longest attenuation length, meaning it is the least absorptive, whereas the heavier Rb<sub>2</sub>CuX<sub>3</sub> analogs have better absorption properties. However, Rb is intrinsically radioactive (a beta emitter), which significantly limits the useful size of Rb<sub>2</sub>CuX<sub>3</sub> crystals for spectroscopy applications. For example, at a density of 3.83 g/cm<sup>3</sup>, we estimate that a Rb<sub>2</sub>CuBr<sub>3</sub> crystal would have an intrinsic activity of 1193 Bq/cm<sup>3</sup>. By comparison, a NaI(Tl) crystal (comparable density and attenuation

length) with dimensions 5 x 10 x 40 cm<sup>3</sup> sees a natural background (at ORNL) of about 900 Bq, making its observed background rate about 0.5 Bg/cm<sup>3</sup>.

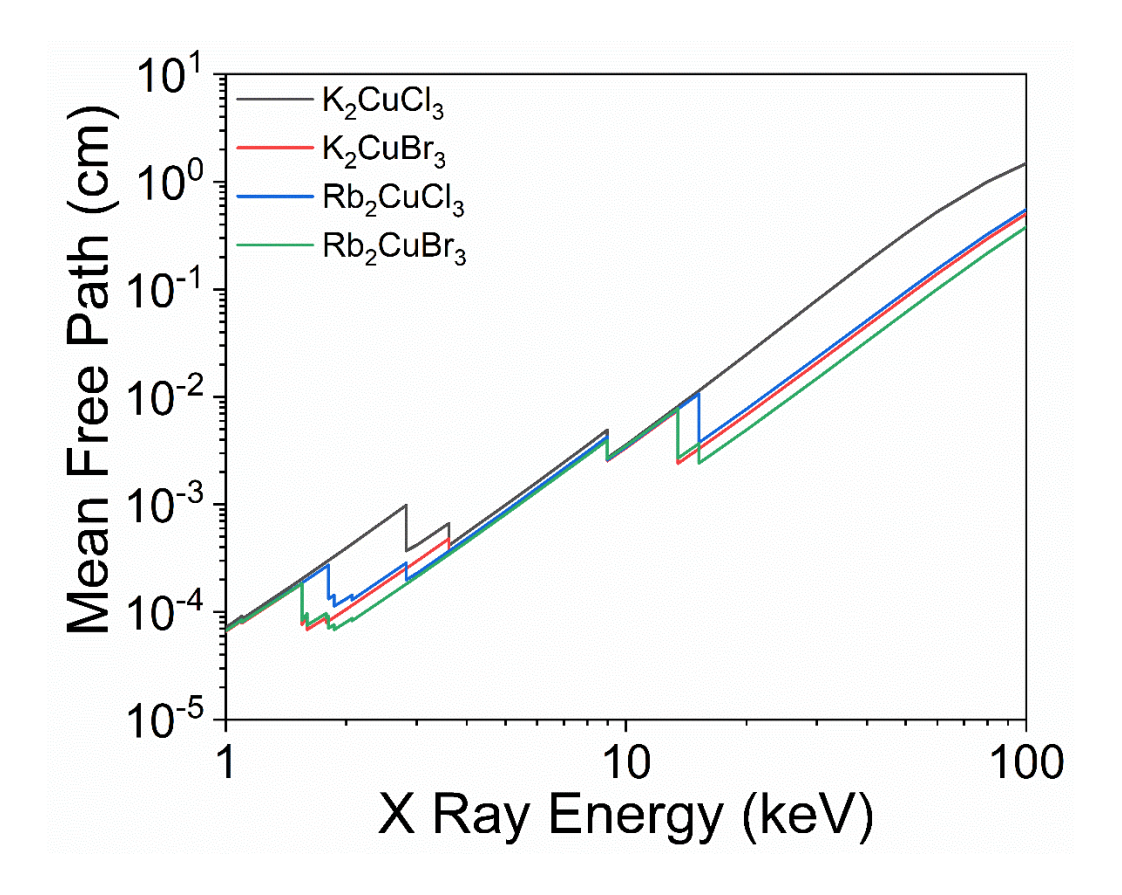


**Figure 4.** Calculated mean free path of photons in K<sub>2</sub>CuCl<sub>3</sub> (black), K<sub>2</sub>CuBr<sub>3</sub> (red), Rb<sub>2</sub>CuCl<sub>3</sub> (blue), and Rb<sub>2</sub>CuBr<sub>3</sub> (green). Sharp breaks correspond to the K and L edges in the constituent atoms.

In medical applications, the bremsstrahlung end point energy is often not more than 100 keV, which puts the most probable emitted X ray between 20 and 50 keV. At these energies and below, compacts and crystals need not be thicker than 1 mm for efficient absorption of the X rays. Since the photoelectric effect is the dominant process at these energies, electrons ejected from atoms will

have energies ~10 keV lower than the ionizing photon. The range of 40 keV electrons in the material becomes the important parameter determining the skin depth that defines the region of total energy deposition. Electrons originating closer to the surface than the range of 40 keV electrons have a high probability of not depositing their full energy in the detector. Using the NIST ESTAR code <sup>61</sup>, we estimate the continuous slowing down approximation (CSDA) range of these electrons to be 15.8 μm, making the totally absorbing thickness of a 1 mm thick detector at least 0.97 mm. We write "at least" here because CSDA range assumes a straight-line path for the electron, whereas in reality, electrons suffer many large-angle scatterings because the primary scatterers are other electrons. Therefore, we conclude that K<sub>2</sub>CuCl<sub>3</sub> should be a viable detector material for medical applications.

The ranges of 1 - 2 MeV electrons and gamma rays (typical energies from terrestrial radioactive sources) are large,  $\sim$ 2.2 - 4.8 mm (CSDA) and  $\sim$ 5 cm (mfp), respectively, necessitating the use of transparent single crystals because pressed polycrystalline compacts thicker than 0.5 - 1 mm are opaque to the RL emission. The heavier halides members of this family will be more likely to find use in high-energy gamma ray detectors because of their higher average atomic number and densities. It will be necessary to produce larger single crystals (at least 5 mm  $\times$  5 mm  $\times$  5 mm) to measure the light yield (number of scintillation photons/deposited MeV) with monoenergetic X or gamma ray sources. Thus, our preliminary investigations of radiation detection properties of K<sub>2</sub>CuX<sub>3</sub> have highlighted the potential of this family for further, more in-depth studies.

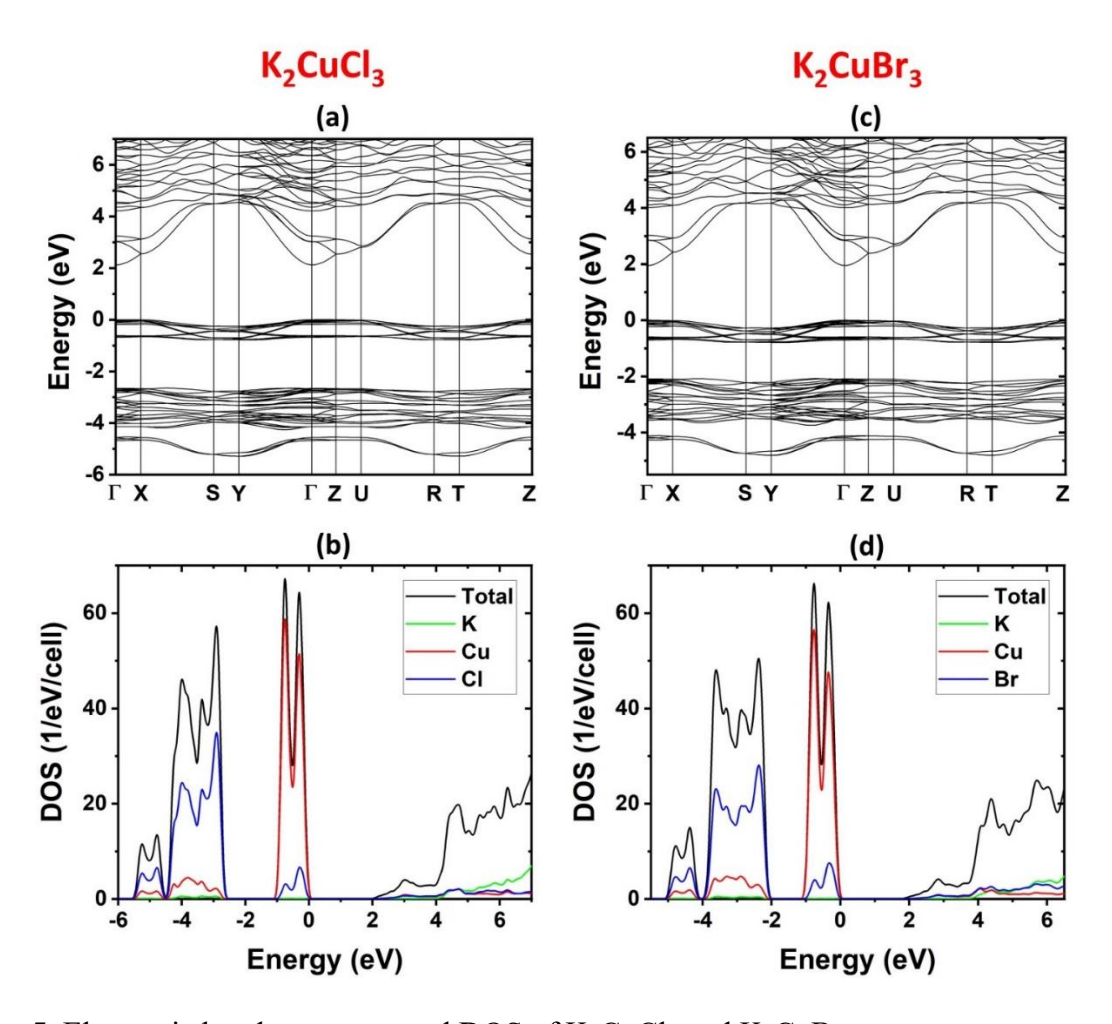
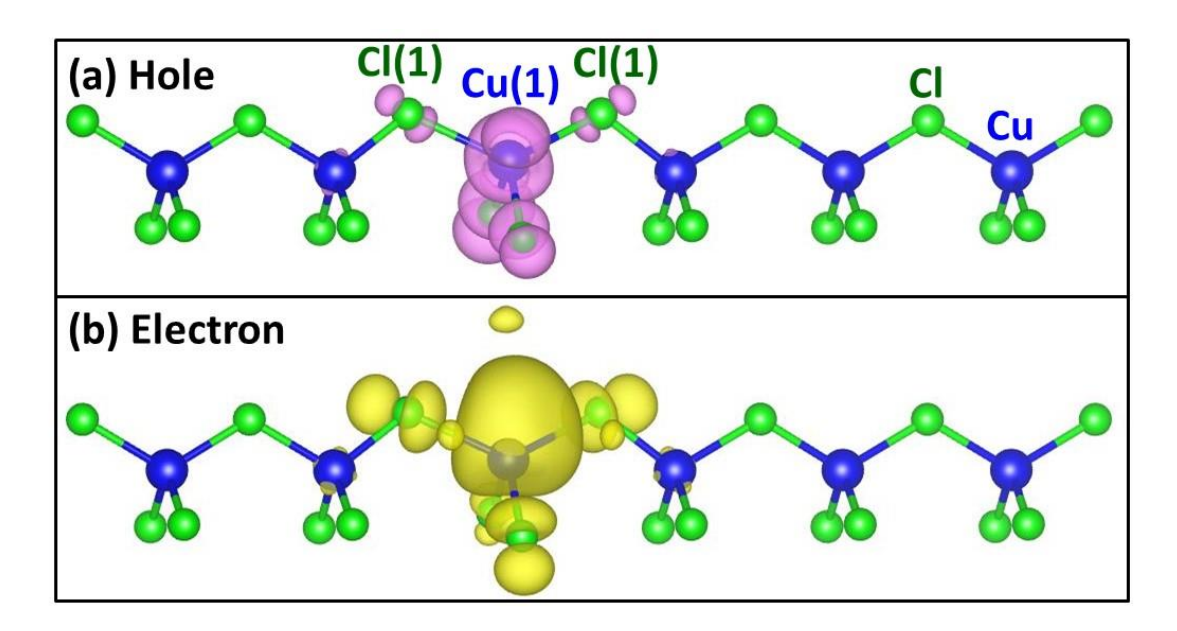


Figure 5. Electronic band structures and DOS of K<sub>2</sub>CuCl<sub>3</sub> and K<sub>2</sub>CuBr<sub>3</sub>.

The electronic band structures of K<sub>2</sub>CuX<sub>3</sub> (X = Cl, Br) are shown in Figure 5. Both compounds exhibit direct band gaps at the Γ point. The PBE-calculated band gaps of K<sub>2</sub>CuCl<sub>3</sub> and K<sub>2</sub>CuBr<sub>3</sub> are 2.13 eV and 1.95 eV, respectively. These PBE band gaps are expected to be underestimated due to the well-known band gap error in the PBE calculation. The hybrid PBE0 calculations increase the band gaps of K<sub>2</sub>CuCl<sub>3</sub> and K<sub>2</sub>CuBr<sub>3</sub>to 4.63 eV and 4.32 eV, respectively. The DOS plots in Figure 5 show that the valence (conduction) band is primarily derived from the Cu-3d (Cu-4s) orbitals hybridized with halogen p orbitals. Since both the conduction and valence band edges are dominated by Cu states, the calculated band gaps are weakly dependent on the halogen.



**Figure 6**. The partial charge density contours of the hole (a) and the electron (b) in the exciton in K<sub>2</sub>CuCl<sub>3</sub>. The Cu and Cl atoms are represented by blue and green balls, respectively. The charge density at the isodensity surface is 0.001 e/bohr<sup>3</sup>.

To understand the origin of the optical emission in K<sub>2</sub>CuX<sub>3</sub>, we calculated the excitonic properties in K<sub>2</sub>CuCl<sub>3</sub>. Despite the dispersive conduction band, the localization of an exciton is found to be strong, leading to significant local structural distortion, which in turn traps the exciton, forming a STE. A STE is centered at a Cu ion, causing elongation of the two adjacent Cu-Cl bonds [Cu(1)-Cl(1) and Cu(1)-Cl(2) in Figure 6] along the 1D chain direction from 2.41 Å to 2.68 Å (a 11% increase). The partial charge density contours of the hole and electron in a STE are shown in Figure 6b. The binding energy of the STE (relative to a pair of free electron and hole) in K<sub>2</sub>CuCl<sub>3</sub> is calculated to be 1.06 eV. The calculated STE emission energy is 2.85 eV, in reasonable agreement with the experimental value of 3.16 eV (392 nm) and the observed RL peak at 3.07 eV (404 nm). These results suggest the STE as the origin of the observed emission in K<sub>2</sub>CuCl<sub>3</sub>. The observed optical emission in K<sub>2</sub>CuBr<sub>3</sub> is similar to that in K<sub>2</sub>CuCl<sub>3</sub>, indicating the same emission mechanism.

#### **CONCLUSION**

In summary, we report preparation and optical properties of all-inorganic copper halides K<sub>2</sub>CuX<sub>3</sub> (X=Cl, Br). K<sub>2</sub>CuX<sub>3</sub> demonstrate narrow blue emission with FWHM values of ~50 nm, very high PLQY values up to unity, and relatively small Stokes shifts for this class of materials. Interestingly, the measured optical properties of K<sub>2</sub>CuX<sub>3</sub> show very weak dependence on A site or X site substitutions. Our computational investigations suggest that both the conduction and valence band edges are primarily made of Cu states, which explains the weak dependence of the observed optical properties on the halogen and alkali metal. Based on our combined experimental and computational work, the blue emission in K<sub>2</sub>CuX<sub>3</sub> is attributed to excitons localized within the  ${}^{1}_{\infty}$ [CuX<sub>3</sub>]<sup>2-</sup> chains centered at a copper ion. Importantly, K<sub>2</sub>CuX<sub>3</sub> are found to exhibit significantly improved air- and photo-stability compared to other analogous copper halides. K<sub>2</sub>CuCl<sub>3</sub> also exhibits radioluminescence at a wavelength similar to the blue emission from PL when exposed to bremsstrahlung X-rays. The combination of inexpensive and earth-abundant chemical composition, high efficiency blue emission and much improved stability of K<sub>2</sub>CuX<sub>3</sub> makes these compounds attractive for consideration for practical optical and radiation detection applications.

#### ASSOCIATED CONTENT

### **Supporting Information.**

Sample photos, powder X-ray diffraction results, DSC/TGA, and comparison of ground samples versus single crystals PL, photos of the RL apparatus.

**AUTHOR INFORMATION** 

**Corresponding Author** 

\*E-mail: saparov@ou.edu

**Notes** 

The authors declare no competing financial interest.

**Author Contributions** 

The manuscript was written through contributions of all authors. All authors have given approval

to the final version of the manuscript. T.C. and M.M prepared the samples, performed PXRD,

TGA/DSC measurements, T.C. performed and analyzed the optical measurements, Z.B. collected

and analyzed radioluminescence data, M-H.D. carried out the theoretical calculations, and B.S.

conceived and supervised the work.

ACKNOWLEDGMENT

We acknowledge the financial support for this work provided by a grant from Oklahoma Center

for the Advancement of Science and Technology (OCAST AR18-008). This material is based

upon work supported by the National Aeronautics and Space Administration under Agreement

No 80NSSC19M0140 issued through NASA Oklahoma EPSCoR. M. H. Du was supported by

the U. S. Department of Energy, Office of Science, Basic Energy Sciences, Materials Sciences

and Engineering Division. We thank Dr. Douglas R. Powell for his help with the single crystal

X-ray diffraction measurements (supported by NSF grant CHE-1726630), Dr. Pawan Kumar for

his helpful tips and Mr. Benjamin Jenson for this assistance with synthesis experiments.

24

#### **REFERENCES**

- 1. Zhang, Q.; Yin, Y., All-inorganic metal halide perovskite nanocrystals: opportunities and challenges. *ACS central science* **2018**, *4* (6), 668-679.
- 2. Li, S.; Luo, J.; Liu, J.; Tang, J., Self-Trapped Excitons in All-Inorganic Halide Perovskites: Fundamentals, Status, and Potential Applications. *The Journal of Physical Chemistry Letters* **2019**, *10* (8), 1999-2007.
- 3. Ghosh, S.; Pradhan, B., Lead-Free Metal Halide Perovskite Nanocrystals: Challenges, Applications, and Future Aspects. *ChemNanoMat* **2019**, *5* (3), 300-312.
- 4. Du, P.; Luo, L.; Cheng, W., Neoteric Mn2+-activated Cs3Cu2I5 dazzling yellow-emitting phosphors for white-LED. *Journal of the American Ceramic Society* **2020**, *103* (2), 1149-1155
- 5. Luo, Z.; Li, Q.; Zhang, L.; Wu, X.; Tan, L.; Zou, C.; Liu, Y.; Quan, Z., 0D Cs3Cu2X5 (X= I, Br, and Cl) Nanocrystals: Colloidal Syntheses and Optical Properties. *Small* **2020**, *16* (3), 1905226.
- 6. Yang, B.; Yin, L.; Niu, G.; Yuan, J. H.; Xue, K. H.; Tan, Z.; Miao, X. S.; Niu, M.; Du, X.; Song, H., Lead-Free Halide Rb2CuBr3 as Sensitive X-Ray Scintillator. *Advanced Materials* **2019**, *31* (44), 1904711.
- 7. Zhang, X.; Wang, H.; Wang, S.; Hu, Y.; Liu, X.; Shi, Z.; Colvin, V. L.; Wang, S.; Yu, W. W.; Zhang, Y., Room Temperature Synthesis of All Inorganic Lead-Free Zero-Dimensional Cs4SnBr6 and Cs3KSnBr6 Perovskites. *Inorganic Chemistry* **2020**, *59* (1), 533-538.
- 8. Lin, R.; Guo, Q.; Zhu, Q.; Zhu, Y.; Zheng, W.; Huang, F., All-Inorganic CsCu2I3 Single Crystal with High-PLQY (≈ 15.7%) Intrinsic White-Light Emission via Strongly Localized 1D Excitonic Recombination. *Advanced Materials* **2019**, *31* (46), 1905079.
- 9. Creason, T. D.; Yangui, A.; Roccanova, R.; Strom, A.; Du, M. H.; Saparov, B., Rb2CuX3 (X=Cl, Br): 1D All-Inorganic Copper Halides with Ultrabright Blue Emission and Up-Conversion Photoluminescence. *Advanced Optical Materials* **2020**, *8* (2), 1901338.
- 10. Li, T.; Mo, X.; Peng, C.; Lu, Q.; Qi, C.; Tao, X.; Ouyang, Y.; Zhou, Y., Distinct green electroluminescence from lead-free CsCuBr 2 halide micro-crosses. *Chemical Communications* **2019**, *55* (31), 4554-4557.
- 11. Zhou, L.; Liao, J. F.; Huang, Z. G.; Wei, J. H.; Wang, X. D.; Li, W. G.; Chen, H. Y.; Kuang, D. B.; Su, C. Y., A Highly Red-Emissive Lead-Free Indium-Based Perovskite Single Crystal for Sensitive Water Detection. *Angewandte Chemie International Edition* **2019**, *58* (16), 5277-5281.
- 12. Zhou, C.; Lin, H.; Tian, Y.; Yuan, Z.; Clark, R.; Chen, B.; van de Burgt, L. J.; Wang, J. C.; Zhou, Y.; Hanson, K., Luminescent zero-dimensional organic metal halide hybrids with near-unity quantum efficiency. *Chemical science* **2018**, *9* (3), 586-593.
- 13. Zhang, R.; Mao, X.; Zheng, D.; Yang, Y.; Yang, S.; Han, K., A Lead-Free All-Inorganic Metal Halide with Near-Unity Green Luminescence. *Laser & Photonics Reviews*, 2000027.
- 14. Zhou, C.; Lin, H.; Shi, H.; Tian, Y.; Pak, C.; Shatruk, M.; Zhou, Y.; Djurovich, P.; Du, M. H.; Ma, B., A zero-dimensional organic seesaw-shaped tin bromide with highly efficient strongly stokes-shifted deep-red emission. *Angewandte Chemie International Edition* **2018**, *57* (4), 1021-1024.

- 15. Majher, J. D.; Gray, M. B.; Strom, T. A.; Woodward, P. M., Cs2NaBiCl6: Mn2+—A New Orange-Red Halide Double Perovskite Phosphor. *Chemistry of Materials* **2019**, *31* (5), 1738-1744.
- 16. Bi, C.; Wang, S.; Kershaw, S. V.; Zheng, K.; Pullerits, T.; Gaponenko, S.; Tian, J.; Rogach, A. L., Spontaneous Self-Assembly of Cesium Lead Halide Perovskite Nanoplatelets into Cuboid Crystals with High Intensity Blue Emission. *Advanced Science* **2019**, *6* (13), 1900462.
- 17. Jun, T.; Sim, K.; Iimura, S.; Sasase, M.; Kamioka, H.; Kim, J.; Hosono, H., Lead-Free Highly Efficient Blue-Emitting Cs3Cu2I5 with 0D Electronic Structure. *Advanced Materials* **2018**, *30* (43), 1804547.
- 18. Morad, V.; Shynkarenko, Y.; Yakunin, S.; Brumberg, A.; Schaller, R. D.; Kovalenko, M. V., Disphenoidal Zero-Dimensional Lead, Tin, and Germanium Halides: Highly Emissive Singlet and Triplet Self-Trapped Excitons and X-ray Scintillation. *Journal of the American Chemical Society* **2019**, *141* (25), 9764-9768.
- 19. Zhou, C.; Lin, H.; Worku, M.; Neu, J.; Zhou, Y.; Tian, Y.; Lee, S.; Djurovich, P.; Siegrist, T.; Ma, B., Blue emitting single crystalline assembly of metal halide clusters. *Journal of the American Chemical Society* **2018**, *140* (41), 13181-13184.
- 20. Xing, J.; Zhao, Y.; Askerka, M.; Quan, L. N.; Gong, X.; Zhao, W.; Zhao, J.; Tan, H.; Long, G.; Gao, L., Color-stable highly luminescent sky-blue perovskite light-emitting diodes. *Nature communications* **2018**, *9* (1), 1-8.
- 21. Gong, X.; Voznyy, O.; Jain, A.; Liu, W.; Sabatini, R.; Piontkowski, Z.; Walters, G.; Bappi, G.; Nokhrin, S.; Bushuyev, O., Electron–phonon interaction in efficient perovskite blue emitters. *Nature materials* **2018**, *17* (6), 550-556.
- 22. Bi, C.; Wang, S.; Li, Q.; Kershaw, S. V.; Tian, J.; Rogach, A. L., Thermally stable copper (II)-Doped cesium lead halide perovskite quantum dots with strong blue emission. *The journal of physical chemistry letters* **2019**, *10* (5), 943-952.
- 23. Steckel, J. S.; Zimmer, J. P.; Coe-Sullivan, S.; Stott, N. E.; Bulović, V.; Bawendi, M. G., Blue luminescence from (CdS) ZnS core–shell nanocrystals. *Angewandte Chemie International Edition* **2004**, *43* (16), 2154-2158.
- 24. Wang, L.; Nagesha, D. K.; Selvarasah, S.; Dokmeci, M. R.; Carrier, R. L., Toxicity of CdSe nanoparticles in Caco-2 cell cultures. *Journal of nanobiotechnology* **2008**, *6* (1), 11.
- 25. Zhang, R.; Mao, X.; Zheng, D.; Yang, Y.; Yang, S.; Han, K., A Lead-Free All-Inorganic Metal Halide with Near-Unity Green Luminescence. *Laser & Photonics Reviews* **2020**, *14* (5), 2000027.
- 26. Zhao, X.; Niu, G.; Zhu, J.; Yang, B.; Yuan, J. H.; Li, S.; Gao, W.; Hu, Q.; Yin, L.; Xue, K. H.; Lifshitz, E.; Miao, X.; Tang, J., All-Inorganic Copper Halide as a Stable and Self-Absorption-Free X-ray Scintillator. *J Phys Chem Lett* **2020**, *11* (5), 1873-1880.
- 27. Yang, B.; Yin, L.; Niu, G.; Yuan, J.-H.; Xue, K.-H.; Tan, Z.; Miao, X.-S.; Niu, M.; Du, X.; Song, H.; Lifshitz, E.; Tang, J., Lead-Free Halide Rb2CuBr3 as Sensitive X-Ray Scintillator. *Advanced Materials* **2019**, *31* (44), 1904711.
- 28. Roccanova, R.; Yangui, A.; Nhalil, H.; Shi, H.; Du, M.-H.; Saparov, B., Near-Unity Photoluminescence Quantum Yield in Blue-Emitting Cs3Cu2Br5–xIx  $(0 \le x \le 5)$ . *ACS Applied Electronic Materials* **2019**, *1* (3), 269-274.
- 29. Roccanova, R.; Yangui, A.; Seo, G.; Creason, T. D.; Wu, Y.; Kim, D. Y.; Du, M.-H.; Saparov, B., Bright Luminescence from Nontoxic CsCu2X3 (X = Cl, Br, I). *ACS Materials Letters* **2019**, *1* (4), 459-465.

- 30. Li, Q.; Chen, Z.; Yang, B.; Tan, L.; Xu, B.; Han, J.; Zhao, Y.; Tang, J.; Quan, Z., Pressure-Induced Remarkable Enhancement of Self-Trapped Exciton Emission in One-Dimensional CsCu2I3 with Tetrahedral Units. *Journal of the American Chemical Society* **2020**, *142* (4), 1786-1791.
- 31. Kresse, G.; Furthmüller, J., Efficiency of ab-initio total energy calculations for metals and semiconductors using a plane-wave basis set. *Computational Materials Science* **1996**, *6* (1), 15-50.
- 32. Kresse, G.; Joubert, D., From ultrasoft pseudopotentials to the projector augmented-wave method. *Physical Review B* **1999**, *59* (3), 1758.
- 33. Perdew, J. P.; Burke, K.; Ernzerhof, M., Generalized gradient approximation made simple. *Physical review letters* **1996**, *77* (18), 3865.
- 34. Perdew, J. P.; Emzerhof, M.; Burke, K., Rationale for mixing exact exchange with density functional approximations. *Journal of Chemical Physics* **1996**, *105* (22), 9982-9985.
- 35. Heyd, J.; Scuseria, G. E.; Ernzerhof, M., Hybrid functionals based on a screened Coulomb potential. *Journal of Chemical Physics* **2003**, *118* (18), 8207-8215.
- 36. Paier, J.; Marsman, M.; Hummer, K.; Kresse, G.; Gerber, I. C.; Angyan, J. G., Screened hybrid density functionals applied to solids. *Journal of Chemical Physics* **2006**, *124* (15).
- 37. Du, M.-H.; Zhang, S. B., Impurity-bound small polarons in ZnO: Hybrid density functional calculations. *Physical Review B* **2009**, *80* (11), 115217.
- 38. Janotti, A.; Varley, J. B.; Choi, M.; Van de Walle, C. G., Vacancies and small polarons in SrTiO3. *Physical Review B* **2014**, *90* (8), 085202.
- 39. Janotti, A.; Franchini, C.; Varley, J. B.; Kresse, G.; Van de Walle, C. G., Dual behavior of excess electrons in rutile TiO2. *physica status solidi (RRL) Rapid Research Letters* **2013**, 7 (3), 199-203.
- 40. Bjaalie, L.; Ouellette, D. G.; Moetakef, P.; Cain, T. A.; Janotti, A.; Himmetoglu, B.; Allen, S. J.; Stemmer, S.; Walle, C. G. V. d., Small hole polarons in rare-earth titanates. *Applied Physics Letters* **2015**, *106* (23), 232103.
- 41. Biswas, K.; Du, M. H., Energy transport and scintillation of cerium-doped elpasolite Cs2LiYCl6: Hybrid density functional calculations. *Physical Review B* **2012**, *86* (1), 014102.
- 42. Jones, R. O.; Gunnarsson, O., The density functional formalism, its applications and prospects. *Reviews of Modern Physics* **1989**, *61* (3), 689-746.
- 43. Görling, A., Density-functional theory beyond the Hohenberg-Kohn theorem. *Physical Review A* **1999**, *59* (5), 3359-3374.
- 44. Hellman, A.; Razaznejad, B.; Lundqvist, B. I., Potential-energy surfaces for excited states in extended systems. *The Journal of Chemical Physics* **2004**, *120* (10), 4593-4602.
- 45. Du, M.-H., Microscopic origin of multiple exciton emission in low-dimensional lead halide perovskites. *The Journal of Chemical Physics* **2019**, *151* (18), 181101.
- Cheng, P.; Sun, L.; Feng, L.; Yang, S.; Yang, Y.; Zheng, D.; Zhao, Y.; Sang, Y.;
   Zhang, R.; Wei, D.; Deng, W.; Han, K., Colloidal Synthesis and Optical Properties of All-Inorganic Low-Dimensional Cesium Copper Halide Nanocrystals. *Angewandte Chemie* 2019, 131 (45), 16233-16237.
- 47. Du, M.-H., Zero-dimensional metal oxide Li4TiO4. *Journal of Materials Chemistry C* **2019**, *7* (19), 5710-5715.

- 48. Shi, H.; Han, D.; Chen, S.; Du, M.-H., Impact of metal ns2 lone pair on luminescence quantum efficiency in low-dimensional halide perovskites. *Physical Review Materials* **2019**, *3* (3), 034604.
- 49. Han, D.; Shi, H.; Ming, W.; Zhou, C.; Ma, B.; Saparov, B.; Ma, Y.-Z.; Chen, S.; Du, M.-H., Unraveling luminescence mechanisms in zero-dimensional halide perovskites. *Journal of Materials Chemistry C* **2018**, *6* (24), 6398-6405.
- 50. Du, M.-H., Emission Trend of Multiple Self-Trapped Excitons in Luminescent 1D Copper Halides. *ACS Energy Letters* **2020**, *5*, 464-469.
- 51. Shannon, R., Revised effective ionic radii and systematic studies of interatomic distances in halides and chalcogenides. *Acta Crystallographica Section A* **1976**, *32* (5), 751-767.
- 52. Saparov, B.; Sun, J.-P.; Meng, W.; Xiao, Z.; Duan, H.-S.; Gunawan, O.; Shin, D.; Hill, I. G.; Yan, Y.; Mitzi, D. B., Thin-film deposition and characterization of a Sn-deficient perovskite derivative Cs2SnI6. *Chemistry of Materials* **2016**, *28* (7), 2315-2322.
- 53. Sharma, M.; Yangui, A.; Whiteside, V. R.; Sellers, I. R.; Han, D.; Chen, S.; Du, M.-H.; Saparov, B., Rb4Ag2BiBr9: A Lead-Free Visible Light Absorbing Halide Semiconductor with Improved Stability. *Inorganic chemistry* **2019**, *58* (7), 4446-4455.
- 54. Biefeld, R. M., The KBr-CuBr and NaBr-CuBr phase diagrams. *Materials Research Bulletin* **1975**, *10* (11), 1151-1156.
- 55. Etter, D. E.; Wiedenheft, C. J., The study of KCl-CuCl eutectic fused salt as a potential intermediate temperature heat transfer and storage medium. *Solar Energy Materials* **1980**, 2 (4), 423-431.
- 56. Zhou, C.; Lin, H.; He, Q.; Xu, L.; Worku, M.; Chaaban, M.; Lee, S.; Shi, X.; Du, M.-H.; Ma, B., Low dimensional metal halide perovskites and hybrids. *Materials Science and Engineering: R: Reports* **2019**, *137*, 38-65.
- 57. Cortecchia, D.; Yin, J.; Bruno, A.; Lo, S.-Z. A.; Gurzadyan, G. G.; Mhaisalkar, S.; Brédas, J.-L.; Soci, C., Polaron self-localization in white-light emitting hybrid perovskites. *Journal of Materials Chemistry C* **2017**, *5* (11), 2771-2780.
- 58. Protesescu, L.; Yakunin, S.; Bodnarchuk, M. I.; Krieg, F.; Caputo, R.; Hendon, C. H.; Yang, R. X.; Walsh, A.; Kovalenko, M. V., Nanocrystals of Cesium Lead Halide Perovskites (CsPbX3, X = Cl, Br, and I): Novel Optoelectronic Materials Showing Bright Emission with Wide Color Gamut. *Nano Letters* **2015**, *15* (6), 3692-3696.
- 59. Ziegler, J. F. INTERACTIONS OF IONS WITH MATTER. http://srim.org/index.htm#HOMETOP (accessed 5/15/20).
- 60. M.J. Berger, J. H. H., S.M. Seltzer, J. Chang, J.S. Coursey, R. Sukumar, D.S. Zucker, and K. Olsen XCOM: Photon Cross Sections Database. https://physics.nist.gov/PhysRefData/Xcom/html/xcom1.html (accessed 5/15/20).
- 61. M.J. Berger, J. S. C., M.A. Zucker and J. Chang Stopping-Power & Range Tables for Electrons, Protons, and Helium Ions.

  <a href="https://physics.nist.gov/PhysRefData/Star/Text/ESTAR.html">https://physics.nist.gov/PhysRefData/Star/Text/ESTAR.html</a> (accessed 5/15/20).

## **TOC Graphic**

